Inorganic Chemistry

Article

pubs.acs.org/IC

Tuning CO_2 Selective Adsorption over N_2 and CH_4 in UiO-67 Analogues through Ligand Functionalization

Bin Wang,[†,‡] Hongliang Huang,[†,§] Xiu-Liang Lv,[†] Yabo Xie,[†] Ming Li,*[,‡] and Jian-Rong Li*[,†,§]

[†]Beijing Key Laboratory for Green Catalysis and Separation and Department of Chemistry and Chemical Engineering, Beijing University of Technology, Beijing 100124, P. R. China

[‡]College of Chemistry and Molecular Engineering, Qing Dao University of Science and Technology, Qingdao 266042, P. R. China

[§]State Key Laboratory of Organic−Inorganic Composites, Beijing University of Chemical Technology, Beijing 100029, P. R. China

Supporting Information

ABSTRACT: Introducing functional groups into pores of metal−organic frameworks (MOFs) through ligand modification provides an efficacious approach for tuning gas adsorption and separation performances of this type of novel porous material. In this work, two UiO-67 analogues, $[Zr_6O_4(OH)_4(FDCA)_6]$ (BUT-10) and $[Zr_6O_4(OH)_4(DTDAO)_6]$ (BUT-11), with functionalized pore surfaces and high stability were synthesized from two functional ligands, 9-fluorenone-2,7-dicarboxylic acid (H_2FDCA) and dibenzo[*b*,*d*]thiophene-3,7-dicarboxylic acid 5,5-dioxide (H_2DTDAO), respectively, and structurally determined by single-crystal X-ray diffraction. Notwithstanding skeleton bend of the two ligands relative to the linear 4,4′-biphenyldicarboxylic acid in UiO-67, the two MOFs have structures similar to that of UiO-67, with only lowered symmetry in their frameworks. Attributed to these additional functional groups (carbonyl and sulfone, respectively) in the ligands, BUT-10 and -11 show enhanced CO_2 adsorption and separation selectivities over N_2 and CH_4, in spite of decreased pore sizes and surface areas compared with UiO-67. At 298 K and 1 atm, the CO_2 uptake is 22.9, 50.6, and 53.5 cm^3/g, and the infinite dilution selectivities of CO_2/CH_4 are 2.7, 5.1, and 9.0 and those of CO_2/N_2 are 9.4, 18.6, and 31.5 for UiO-67, BUT-10, and BUT-11, respectively. The selectivities of CO_2/CH_4 and CO_2/N_2 are thus enhanced 1.9 and 2.0 times in BUT-10 and 3.3 and 3.4 times in BUT-11, respectively, on the basis of UiO-67. The adsorption mechanism of CO_2 in BUT-11 has also been explored through computational simulations. The results show that CO_2 molecules locate around the sulfone groups in pore surfaces of BUT-11, verifying at the molecular level that sulfone groups significantly increase the affinity toward CO_2 molecules of the framework. This provides thus an efficient strategy for the design of CO_2 capture materials.

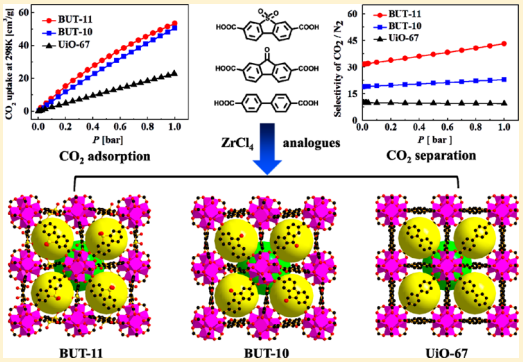

1. INTRODUCTION

Concerns about greenhouse gases in the atmosphere have led to the development of efficient CO_2 capture technologies.[1,2] For the separation of CO_2, adsorption-based methods are promising because of their simple and easy control, low operating and capital costs, and superior energy efficiency.[3] Among the various materials for adsorptive separation, metal−organic frameworks (MOFs), as a new family of porous solids, are attractive because of their large surface areas, adjustable pore sizes, and controllable pore-surface properties. So far, a lot of papers including several excellent reviews have demonstrated the potential application of MOFs in CO_2 capture and storage.[4−8] Nevertheless, one drawback faced by most MOFs for application in CO_2 capture lies in their poor physicochemical stability.[9]

Recently, a zirconium(IV)-based MOF named UiO-66 has attracted intense interest for its excellent stability and good adsorption ability toward some small molecules including CO_2.[10−12] It has been demonstrated that this MOF is thermally stable up to 773 K and its structure remains unaltered toward a wide class of aqueous solvents, in contrast to the majority of MOFs. The hydroxylated form of UiO-66 is constructed from hexanuclear $[Zr_6O_4(OH)_4]$ building units, in which the triangular faces of the Zr_6 octahedron are alternatively capped by μ_3-O and μ_3-OH groups. The Zr_6 polyhedra are interconnected along the edges through carboxylates of 12 1,4-benzenedicarboxylate (BDC) linkers to form a cubic three-dimensional (3D) framework.[10] Some research has shown that the introduction of functional groups such as −COOH, $-SO_3H$, and $-NH_2$ to the BDC ligand could significantly enhance the CO_2 adsorption and separation ability of UiO-66 in either experiments or theoretical calculations.[13−16] For gas adsorptive separation, both the adsorption capacity and selectivity play important roles. Because of smaller pore size and surface area, the introduction of functional groups can significantly reduce the specific surface area of UiO-66, which would lead to a negative effect on its adsorption working capacity.[12,13] UiO-67, the isostructural analogue of UiO-66, is constructed from a longer linker, 4,4′-biphenyldicarboxylate

Received: June 9, 2014
Published: August 12, 2014

   dx.doi.org/10.1021/ic5013473 | *Inorg. Chem.* 2014, 53, 9254−9259

(BPDC), to give larger pore size, being considered as a more promising platform for functional materials with enhanced CO_2 adsorption and separation abilities.[17] However, owing to the larger pore size in UiO-67, the interaction between the CO_2 molecule and the framework is weaker than that in UiO-66. Thus, loading polar functional groups on the BPDC skeleton is a feasible method to increase the adsorption uptake and selectivity of the resulting material toward CO_2. To the best of our knowledge, there are rare reports on the functionalized UiO-67 analogues.[18]

In this work, by employing two functionalized ligands, 9-fluorenone-2,7-dicarboxylic acid (H_2FDCA) and dibenzo[*b*,*d*]-thiophene-3,7-dicarboxylic acid 5,5-dioxide (H_2DTDAO), two UiO-67 analogues, $[Zr_6O_4(OH)_4(FDCA)_6]_n$·S (BUT-10, where BUT = Beijing University of Technology) and $[Zr_6O_4(OH)_4(DTDAO)_6]_n$·S (BUT-11), were synthesized, respectively. Their structures were determined by single-crystal X-ray diffraction. Compared with UiO-67, BUT-10 and -11 show large enhancement of the CO_2 adsorption and selectivity over CH_4 and N_2. It should be pointed out that, during the preparation of this manuscript, CO_2 adsorption of BUT-11 was reported,[18] where powder X-ray diffraction (PXRD) was used to determine its structure and CO_2 adsorption data were provided. Herein, we report the synthesis and crystal structures of BUT-10 and -11, which were characterized by single-crystal X-ray diffraction, as well as a detailed CO_2 adsorption and separation exploration by both experimental characterizations and computational simulations.

2. EXPERIMENTAL SECTION

2.1. Materials and Methods. All general reagents and solvents (AR grade) were commercially available and were used as received. $ZrCl_4$, 4,4′-biphenyldicarboxylic acid (H_2BPDC), and 9-fluorenone-2,7-dicarboxylic acid (H_2FDCA) were purchased from J&K Chemical. Fourier transform infrared (FT-IR) data were recorded on an IRAffinity-1 instrument. PXRD patterns were recorded on a Bruker D8-Focus Bragg−Brentano X-ray powder diffractometer equipped with a copper sealed tube (λ = 1.54178) at room temperature. Simulation of the PXRD spectrum was carried out by the single-crystal data and diffraction-crystal module of the *Mercury* program available free of charge via the Internet at http://www.ccdc.cam.ac.uk/mercury/. Thermogravimetric analysis (TGA) data were obtained on a TGA-50 (Shimadzu) thermogravimetric analyzer with a heating rate of 2 °C/min under a N_2 atmosphere. Gas adsorption isotherms were measured by a volumetric method using a Micromeritics ASAP2020 surface area and pore analyzer. A high purity grade of gases (99.999% purity) was used throughout the adsorption experiments. P_0 is the saturation pressure at given temperature of the respective gas. For activation of the samples, the as-synthesized sample was soaked in fresh *N*,*N*-dimethylformamide (DMF) for 24 h, and the extract was discarded. Fresh acetone was subsequently added, and the sample was allowed to remain in it for 24 h. This procedure was again repeated two times. After the acetone extract was decanted, the sample was dried under a dynamic vacuum ($<10^{-3}$ Torr) at room temperature for 1 h. Before adsorption measurement, the sample was further activated using the "outgas" function of the adsorption analyzer for 10 h at 80 °C.

2.2. Syntheses. The ligand dibenzo[*b*,*d*]thiophene-3,7-dicarboxylic acid 5,5-dioxide (H_2DTDAO)[19] and UiO-67[20] were synthesized according to the literature methods.

$[Zr_6O_4(OH)_4(FDCA)_6]_n$·S (BUT-10; S = Nonassignable Solvent Molecules). A solution of H_2FDCA (80 mg, 0.3 mmol), $ZrCl_4$ (71 mg, 0.3 mmol), and 3 mL of acetic acid (HOAc) in 17 mL of DMF was sealed in a 20 mL glass vial and heated at 120 °C for 10 h. The resulting yellow crystals were collected and washed with DMF and acetone and then dried in air (yield: 49 mg). For PXRD of the as-synthesized material, TGA, and FT-IR, see Figures S1−S3 in the experimental section of the Supporting Information (SI), respectively.

$[Zr_6O_4(OH)_4(DTDAO)_6]_n$·S (BUT-11). A solution of H_2DTDAO (61 mg, 0.2 mmol), $ZrCl_4$ (47 mg, 0.2 mmol), and 1.7 mL of trifluoroacetic acid in 18 mL of DMF was sealed in a 20 mL glass vial and heated at 120 °C for 48 h. The resulting colorless crystals were collected and washed with DMF and acetone and then dried in air (yield: 35 mg). For PXRD of as-synthesized material, TGA, and FT-IR, see Figures S1−S3 in the experimental section of the SI, respectively.

2.3. Single-Crystal X-ray Diffraction. The diffraction data of BUT-10 were collected on a Bruker-AXS APEX-II CCD X-ray diffractometer equipped with graphite-monochromated Mo Kα radiation (λ = 0.71073 Å) at 173 K. Raw data collection and reduction were done using *APEX2* software.[21] Absorption corrections were applied using the *SADABS* routine.[22] The diffraction data of BUT-11 were collected on an Agilent Supernova CCD diffractometer equipped with graphite-monochromated Cu Kα radiation (λ = 1.54184 Å) at 173 K. The data sets were corrected by empirical absorption correction using spherical harmonics, implemented in the *SCALE3 ABSPACK* scaling algorithm.[23] The structures of BUT-10 and -11 were solved by direct methods and refined by full-matrix least squares on F^2 with anisotropic displacement using the *SHELXTL* software package.[24] Non-H atoms were refined with anisotropic displacement parameters during the final cycles. H atoms of ligands were calculated in ideal positions with isotropic displacement parameters. Those in the OH groups of the zirconium(IV)-based clusters were not added but were calculated into the molecular formula of the crystal data. There are large solvent-accessible pore volumes in the crystals of BUT-10 and -11, which are occupied by highly disordered solvent molecules. No satisfactory disorder model for these solvent molecules could be achieved, and therefore the *SQUEEZE* program implemented in *PLATON* was used to remove the electron densities of these disordered species.[25] Thus, all of the electron densities from free solvent molecules have been "squeezed" out. The details of structural refinement can be found in Tables S1 and S2 and the CIF files in the SI.

2.4. Fitting of Pure-Component Isotherms. The pure-component CO_2, CH_4, and N_2 adsorption isotherm data measured at 298 K were fitted with the dual-site Langmuir model

$$N = N_1^{\max}\frac{b_1 p}{1 + b_1 p} + N_2^{\max}\frac{b_2 p}{1 + b_2 p}$$

where p is the pressure of the bulk gas at equilibrium with the adsorbed phase (kPa), N is the adsorbed amount per mass of adsorbent (mol/kg), $N_1^{\max}$ and $N_2^{\max}$ are the saturation capacities of sites 1 and 2 (mol/kg), and b_1 and b_2 are the affinity coefficients of sites 1 and 2 (kPa^{-1}).

2.5. Isosteric Heat of Adsorption. The isosteric heat of adsorption represents the strength of the interactions between adsorbate molecules and the adsorbent lattice atoms and can be used as a measurement of the energetic heterogeneity of a solid surface. The isosteric heat of adsorption at a given amount can be calculated by the Clausius−Clapeyron equation as

$$Q_{st} = -RT^2\left(\frac{\partial \ln P}{\partial T}\right)_{n_a}$$

where Q_{st} is the isosteric heat of adsorption (kJ/mol), P is the pressure (kPa), T is the temperature, R is the gas constant, and n_a is the adsorption amount (mmol/g).

2.6. Calculations of the Adsorption Selectivity. The selectivity of preferential adsorption of component 1 over component 2 in a mixture containing 1 and 2 can be formally defined as

$$S_{ads} = \frac{q_1/q_2}{p_1/p_2}$$

In the equation, q_1 and q_2 are the absolute loadings. In all of the calculations to be presented below, the calculations of S_{ads} are based on

dx.doi.org/10.1021/ic5013473 | *Inorg. Chem.* 2014, 53, 9254−9259

the use of the Ideal Adsorbed Solution Theory (IAST) of Myers and Prausnitz.[26] These calculations are carried out using the pure-component isotherm fits of absolute loadings.

3. RESULTS AND DISCUSSION

3.1. Synthesis, Structures, and Pore Characterizations. The optimized geometries of the three ligands used are shown in Figure 1a. It can be seen that a carbonyl group and a sulfone

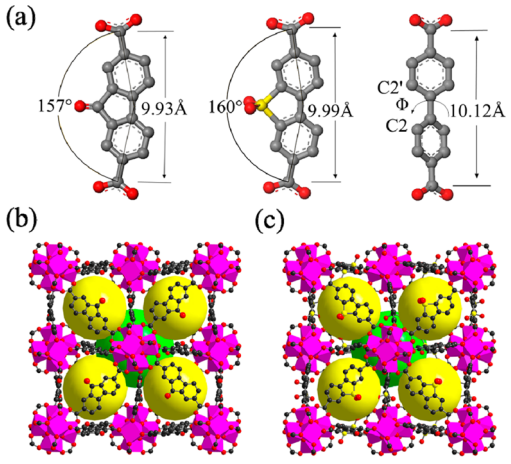

Figure 1. (a) Geometries of the ligands FDCA, DTDAO, and BPDC. (b) Crystal structure of BUT-10. (c) Crystal structure of BUT-11. H atoms on the ligands are omitted for clarity; the large green and yellow spheres represent void regions inside the frameworks. Color code: Zr polyhedra, pink; octahedral cages, green; tetrahedral cages, yellow; C, black gray; O, red; S, yellow.

group are introduced into the BPDC skeleton in FDCA and DTDAO, respectively. These introduced functional groups link C2 and C2′ in BPDC to make the skeleton bent with an angle of 157° and 160°, respectively, and the distance between the two carboxylate groups become slightly shorter compared with that in BPDC. In addition, two benzene rings in FDCA and DTDAO are coplanar, in contrast with an about 31° dihedral angle in BPDC. It is interesting that, even with changes of these structural parameters in the ligands, the framework structures of their Zr-MOFs are similar, as described below. This provides a good platform for exploring the effects of the functional groups in ligands on the gas adsorption performances of the resulting MOFs.

The reaction of the two functional ligands with $ZrCl_4$ in DMF at 120 °C yielded two MOFs, BUT-10 and -11, as single crystals, respectively. It should be pointed out that, during the synthesis of the zirconium-based MOFs, a modular acid is crucial, particularly for obtaining a single-crystal sample. In our case, acetic acid and trifluoroacetic acid were used, respectively, to obtain MOF crystals big enough for single-crystal X-ray diffraction. It has been reported that BUT-11 can also be obtained in microcrystal form when using HCl or AcOH as a modular.[18] In the case when HCl was used, it was found that Cl^- ions could provide charge compensation to the Zr-MOF structures, which makes the structure break down incompletely.[27]

As shown in Figure S2 in the SI, BUT-10 and -11 are thermally stable up to 500 and 420 °C, respectively, being slightly lower than that of UiO-67 (decomposition at 520 °C). Clearly, the functionalization of the ligand led to a change of the coordination bond strength, which finally affected the materials' thermal stability. After removal of the solvent molecules from the as-synthesized samples, the frameworks of BUT-10 and -11 remained intact, as confirmed by PXRD (Figure S1 in the SI).

Single-crystal X-ray diffraction analysis reveals that the structures of BUT-10 and -11 were constructed by hexanuclear $[Zr_6O_4(OH)_4]$ building units interconnected through carboxylate groups of 12 organic linkers to form 3D frameworks (Figure 1b,c). Obviously, the two MOFs share the same structure with UiO-67 even though of lower symmetry [crystallized in the lower space group of $Pa\bar{3}$ compared with that ($Fm\bar{3}m$) of UiO-67] because of the geometric change of the ligands. This result proves that the structures of MOFs can be tolerant in a certain degree change of ligands in some systems. In their frameworks, there exist two types of polyhedral cages, octahedral and tetrahedral (Figures S5 and S6 in the SI). Their sizes across respective edges are 19.16, 18.42, and 18.54 Å for UiO-67, BUT-10, and BUT-11, respectively. After removal of free solvent molecules, the total solvent-accessible volumes of these three frameworks are estimated to be 68.1, 64.0, and 63.4%, respectively, by *PLATON*.

In order to evaluate the permanent porosity of the two MOFs, N_2 adsorption experiments were performed at 77 K. For comparison, N_2 adsorption of UiO-67 was also measured under similar conditions. As shown in Figure 2, the three MOFs gave

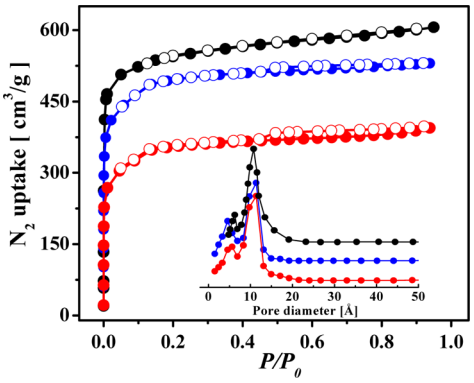

Figure 2. N_2 sorption isotherms of UiO-67 (black), BUT-10 (blue), and BUT-11 (red) at 77 K (filled and open symbols represent adsorption and desorption data, respectively). Inset: density functional theory pore-size distributions for the three MOFs determined from their N_2 adsorption isotherms at 77 K.

basically type I isotherms, being characteristic of microporous materials. Small stepwise adsorption and hysteresis observed in BUT-10 and -11 could be attributed to cage-shape pores in their frameworks.[28] The evaluated Brunauer–Emmett–Teller (S_{BET}) and Langmuir surface areas ($S_{Langmuir}$) from the N_2 adsorption isotherms are 2505 and 3040, 1848 and 2185, and 1310 and 1571 m^2/g for UiO-67, BUT-10, and BUT-11, respectively. The maximum N_2 adsorptions (at $P/P_0 = 0.95$) of 606, 531, and 398 cm^3/g suggest pore volumes of 1.10, 0.82, and 0.62 cm^3/g for UiO-67, BUT-10, and BUT-11, respectively. It is clear that the introduction of functional groups in the ligands decreased the pore sizes and surface areas of the resulting MOFs. The pore-size distributions are also consistent with the crystal structure determination (Figure 2, inset).

3.2. CO_2 Selective Adsorption. The adsorption isotherms of pure CO_2, CH_4, and N_2 in the evacuated UiO-67, BUT-10, and BUT-11, respectively, were experimentally measured, and

dx.doi.org/10.1021/ic5013473 | Inorg. Chem. 2014, 53, 9254–9259

the results are shown in Figures 3 (at 298 K) and S4 in the SI (at 273 K). As can be seen from these isotherm data, the three

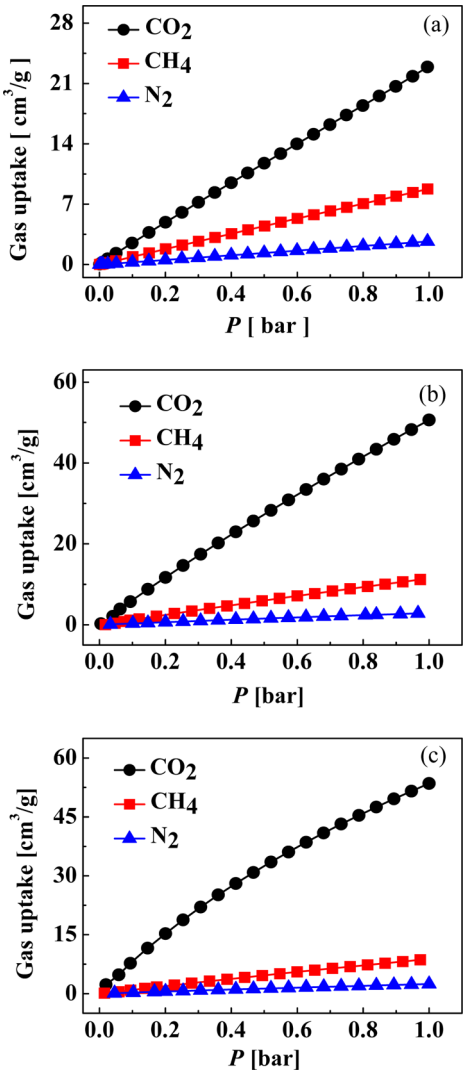

Figure 3. CO_2, CH_4, and N_2 adsorption isotherms at 298 K for (a) UiO-67, (b) BUT-10, and (c) BUT-11.

MOFs have a maximum CO_2 uptake of 22.9, 50.6, and 53.5 cm^3/g at 298 K and 1 atm, CH_4 uptake of 8.7, 11.4, and 8.8 cm^3/g, and N_2 uptake of 2.7, 2.9, and 2.4 cm^3/g. It is quite interesting that the CO_2 uptakes in BUT-10 and -11 are now more than double compared with their parent MOF, UiO-67, demonstrating that added functional groups in the ligands are able to significantly enhance the CO_2 adsorption capacities of the resulting MOFs, even if they have led to decreased pore sizes as mentioned above. In a recent report,[18] the CO_2 uptake at 298 K and 1 atm was 53.1 cm^3/g for the BUT-11 sample obtained using HCl as the modular in the synthesis, being comparable with our result.

The isosteric heats of CO_2 adsorption are calculated based on the adsorption data collected at 273 and 298 K. As shown in Figure 4, the Q_{st} values for BUT-10 and -11 are 21.8−18.9 and 25.9−22.3 kJ/mol, respectively, being higher than that of 15.9−15.8 kJ/mol for UiO-67. The trend in the Q_{st} values is clearly in accordance with the uptake amounts of the order: BUT-11 > BUT-10 > UiO-67.

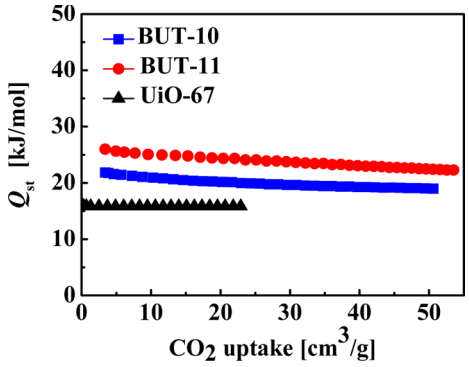

Figure 4. Isosteric heats (Q_{st}) of CO_2 adsorption in UiO-67, BUT-10, and BUT-11.

It is clear that the CO_2 uptake and isosteric heats of BUT-10 and -11 are higher than those of UiO-67, which can be attributed to the stronger interactions between the carbonyl and sulfone groups in the two MOFs and CO_2 molecules. In order to elucidate these observations at the molecular level, grand canonical Monte Carlo (GCMC) simulation was used to evaluate the adsorption properties of BUT-11.[29] As shown in Figure 5, after adsorption snapshots indicate that CO_2

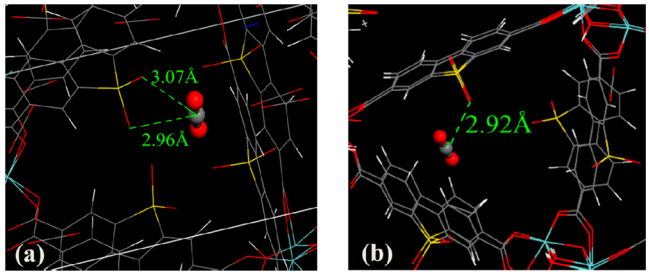

Figure 5. Local view of the snapshots extracted from GCMC simulation at 0.1 bar and 298 K, showing the interactions between the CO_2 molecule and the sulfone group in BUT-11: (a) cross interaction; (b) parallel interaction.

molecules locate around sulfone groups, which shows that there are strong interactions between the CO_2 molecule and the sulfone group in BUT-11. We can also see that there are two types of interaction modes: cross-interaction mode (Figure 5a) and parallel-interaction mode (Figure 5b) for CO_2. In the former mode, the linear O═C═O molecule displays a cross interaction with the O═S═O entity, with the distance between the C atom of CO2 and the two O atoms of the sulfone group being 2.96 and 3.07 Å, respectively. In the latter mode, it displays a parallel interaction with the O═S═O entity, with a distance between the C and O atoms of 2.92 Å. The relatively short distance between the sulfone group and CO_2 molecule implies a strong interaction. Because the CO_2 molecule possesses a large quadrupole moment, the C atom is positively charged, and the O atoms of the sulfone group is negative, the interactions between the O atoms in sulfone and the C atom in CO_2 thus lead to two types of interaction modes. In addition, the radial distribution functions (RDFs) gave the distribution of CO_2 molecules around the sulfone group from the statistics perspective (see Figure S8 in the SI). It was found that the distance between the O atoms in the sulfone group and the C atom in CO_2 is about 3 Å, being in accordance with the snapshot results.

dx.doi.org/10.1021/ic5013473 | Inorg. Chem. 2014, 53, 9254−9259

The enhancement of CO_2 uptakes found in the two functionalized MOFs prompted us to investigate their CO_2 adsorption selectivity over other important gases, including CH_4 and N_2. In order to establish the feasibility of these separations, we performed selectivity calculations using the IAST method.[30−33] To obtain excellent fitting curves, several isotherm models were tested to fit the experimental pure isotherms of CO_2, CH_4, and N_2. For all MOFs, the dual-site Langmuir model was found to be best ($R^2 > 0.9995$; Figure S9 in the SI). The fitted isotherm parameters were used to predict the IAST selectivities of these MOFs. The resulting selectivities for 10:90 CO_2/CH_4 and 15:85 CO_2/N_2 mixtures in the three MOFs as a function of the total bulk pressure are presented in Figure 6. The CO_2/CH_4 selectivities are 2.7−2.9, 5.1−5.2, and

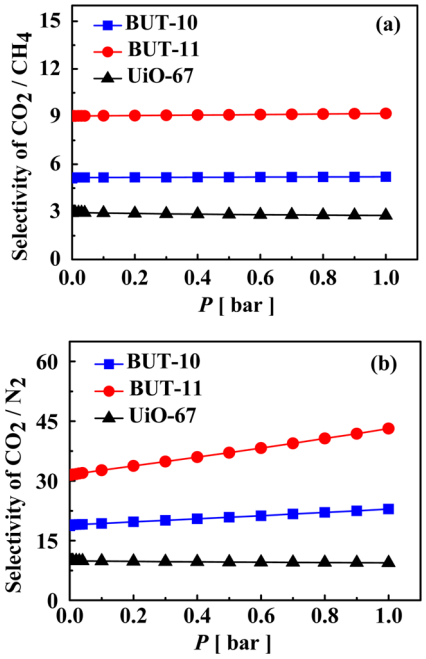

Figure 6. IAST-predicted selectivities toward (a) 10:90 CO_2/CH_4 and (b) 15:85 CO_2/N_2 in UiO-67, BUT-10, and BUT-11, respectively.

9.0−9.2, and the CO_2/N_2 selectivities are 9.4−9.9, 18.6−22.9, and 31.5−43.1 for UiO-67, BUT-10, and BUT-11, respectively. At very low loading, these values are almost identical with the ratios of the Henry constants obtained in the same ranges: 3.1, 6.2, and 9.5 for the CO_2/CH_4 and 9.4, 18.1, and 30.5 for the CO_2/N_2 in UiO-67, BUT-10, and BUT-11, respectively.

The higher CO_2 adsorption enthalpies and selectivities over CH_4 and N_2 in BUT-10 and -11 compared with those of UiO-67 can be attributed to the stronger interactions between the functionalized frameworks and CO_2 molecules. For BUT-11, the primary interaction between CO_2 molecules and the framework should be the electron donor−acceptor effect, in which the O atoms of the sulfone group serve as the electron-donor center and the C atoms of CO_2 as the electron-acceptor center. In addition, the quadrupolar interaction between the sulfone group and CO_2 molecule should also contribute to the observed trend. Accordingly, a similar but weaker electron donor−acceptor interaction may be expected in the CO_2 adsorption by BUT-10 because of the lower electron-donating ability of the carbonyl group compared with the sulfone group.

A lot of MOFs have been checked for the selective adsorption of CO_2 over CH_4 and N_2, and Table 1 lists infinite

Table 1. Infinite Dilution Selectivities of CO_2/CH_4 and CO_2/N_2 in Some Selected MOFs

MOF	T/K	S_{CO_2/CH_4}	S_{CO_2/N_2}	ref
BUT-10	298	5.1	18.6	this work
BUT-11	298	9.0	31.5	this work
UiO-67	298	2.7	9.4	this work
BUT-11(AcOH)	298	6.9	24.1	18
UiO-66(Zr)	298	3.2	13.4	13
UiO-66(Zr)-Br	298	4.7	25.1	13
UiO-66(Zr)-NO_2	298	5.1	26.4	13
UiO-66(Zr)-NH_2	303	9.0		12
UiO-66(Zr)-$(OH)_2$	303	9.0		12
UiO-66(Zr)-$(CF_3)_2$	303	7.5		12
UiO-66(Zr)-SO_3H	303	9.1		12
ZIF-8	298	2.6	8.4	34
ZIF-68	298	5.0	18.0	35
ZIF-69	298	5.2	20.0	35
ZIF-70	298	5.1	17.0	35
ZIF-79	298	6.2	23.0	35
ZIF-81	298	6.3	24.0	35
ZIF-100	298	5.9	25.0	36
ZIF-95	298	4.3	18.0	36
Cu-BTC	298	6.4		37
MOF-5	298	1.8		37
MOF-74(Co)	298		25.0	38
Cu-BTTriex	298		21.0	39
MOF-508b	303	3.0	3.8	40
MIL-101(Cr)	288	6.5	12.6	41
MIL-125-NH_2	298		27.0	42
MIL-68-Al	303	9.0	37.0	43
MIL-47(V)	298	2.0		44

dilution selectivities of CO_2/CH_4 and CO_2/N_2 in BUT-10 and -11 and some selected MOFs. The selectivities in BUT-11 are close to the MOFs with $-NH_2$, $-OH$, and $-SO_3H$ functional groups including UiO-66-X[12] and MIL-125-NH_2,[42] whereas the selectivities in BUT-10 are similar to $-Br$- and $-NO_2$-functionalized MOFs such as UiO-66-Br and $-NO_2$[13] and some ZIFs.[34,35] These results show that both carbonyl and sulfone groups are indeed useful in tailoring MOFs for CO_2 capture and other specific adsorption-based applications.

4. CONCLUSIONS

In summary, two MOFs, BUT-10 and -11, were obtained by using carbonyl- and sulfone-functionalized ligands, respectively, and structurally characterized by single-crystal X-ray diffraction. They have the same structures as UiO-67 even with a lower framework symmetry due to ligand modifications. The introduction of these functional groups has decreased the pore sizes and surface areas of the resulting MOFs but enhanced CO_2 adsorption capacities and selectivities over CH_4 and N_2, compared with UiO-67. In addition, computational simulations were performed to provide a microcosmic mechanism of CO_2 adsorption in BUT-11. Both snapshots and RDFs showed at the molecular level that CO_2 molecules locate around sulfone groups in BUT-11, and there are strong interactions between them. The adsorption selectivities found in BUT-10 and -11 are also comparable to those reported MOFs with functional groups of $-NH_2$, $-OH$, $-Br$, $-NO_2$, and $-SO_3H$. The comparable or relatively high CO_2 adsorption selectivities in BUT-10 and -11 demonstrate that introducing carbonyl and sulfone groups onto the pore surfaces of MOFs

dx.doi.org/10.1021/ic5013473 | Inorg. Chem. 2014, 53, 9254−9259

can significantly increase their affinity toward CO_2 molecules, thereby enhancing the CO_2 capture ability, which provided a strategy for the development of CO_2 capture materials.

■ ASSOCIATED CONTENT

Supporting Information

X-ray crystallographic data in CIF format, details of structure refinement, PXRD, TGA, FT-IR, gas adsorption, additional structural figures, molecular simulation methods, force field details, GCMC simulation, RDFs, and fitting adsorption data. This material is available free of charge via the Internet at http://pubs.acs.org.

■ AUTHOR INFORMATION

Corresponding Authors

*E-mail: liming928@qust.edu.cn.
*E-mail: jrli@bjut.edu.cn.

Notes

The authors declare no competing financial interest.

■ ACKNOWLEDGMENTS

We are thankful for financial support from the Natural Science Foundation of China (Grants 21271015 and 21322601), the Program for New Century Excellent Talents in University (Grant NCET-13-0647), and the Beijing Municipal Natural Science Foundation (Grant 2132013).

■ REFERENCES

(1) Yu, K. M. K.; Curcic, I.; Gabriel, J.; Tsang, S. C. E. *ChemSusChem* **2008**, *1*, 893−899.
(2) Figueroa, J. D.; Fout, T.; Plasynski, S.; McIlvried, H.; Srivastava, R. D. *Int. J. Greenhouse Gas Control* **2008**, *2*, 9−20.
(3) Choi, S.; Drese, J. H.; Jones, C. W. *ChemSusChem* **2009**, *2*, 796−854.
(4) Li, J.-R.; Kuppler, R. J.; Zhou, H.-C. *Chem. Soc. Rev.* **2009**, *38*, 1477−1504.
(5) Düren, T.; Bae, Y.-S.; Snurr, R. Q. *Chem. Soc. Rev.* **2009**, *38*, 1237−1247.
(6) Li, J.-R.; Ma, Y.-G.; McCarthy, M. C.; Sculley, J.; Yu, J.; Jeong, H.-K.; Balbuena, P. B.; Zhou, H.-C. *Coord. Chem. Rev.* **2011**, *255*, 1791−1823.
(7) Li, J.-R.; Sculley, J.; Zhou, H.-C. *Chem. Rev.* **2012**, *112*, 869−932.
(8) Sumida, K.; Rogow, D. L.; Mason, J. A.; McDonald, T. M.; Bloch, E. D.; Herm, Z. R.; Bae, T.; Long, J. R. *Chem. Rev.* **2012**, *112*, 724−781.
(9) Czaja, A. U.; Trukhan, N.; Müller, U. *Chem. Soc. Rev.* **2009**, *38*, 1284−1293.
(10) Cavka, J. H.; Jakobsen, S.; Olsbye, U.; Guillou, N.; Lamberti, C.; Bordiga, S.; Lillerud, K. P. *J. Am. Chem. Soc.* **2008**, *130*, 13850−13851.
(11) Valenzano, L.; Civalleri, B.; Chavan, S.; Bordiga, S.; Nilsen, H. M.; Jakobsen, S.; Lillerud, K. P.; Lamberti, C. *Chem. Mater.* **2011**, *23*, 1700−1718.
(12) Yang, Q.; Wiersum, A. D.; Llewellyn, P. L.; Guillerm, V.; Serre, C.; Maurin, G. *Chem. Commun.* **2011**, *47*, 9603−9605.
(13) Zhang, W.; Huang, H.; Zhong, C.; Liu, D. *Phys. Chem. Chem. Phys.* **2012**, *14*, 2317−2325.
(14) Kim, M.; Cohen, S. M. *CrystEngComm* **2012**, *14*, 4096−4104.
(15) Kandiah, M.; Nilsen, M. H.; Usseglio, S.; Jakobsen, S.; Olsbye, U.; Tilset, M.; Larabi, C.; Quadrelli, E. A.; Bonino, F.; Lillerud, K. P. *Chem. Mater.* **2010**, *22*, 6632−6640.
(16) Foo, M. L.; Horike, S.; Fukushima, T.; Hijikata, Y.; Kubota, Y.; Takata, M.; Kitagawa, S. *Dalton Trans.* **2012**, *41*, 13791−13794.
(17) Yang, Q.; Guillerm, V.; Ragon, F.; Wiersum, A. D.; Llewellyn, P. L.; Zhong, C.; Devic, T.; Serre, C.; Maurin, G. *Chem. Commun.* **2012**, *48*, 9831−9833.
(18) Xydias, P.; Spanopoulos, I.; Klontzas, E.; Froudakis, G. E.; Trikalitis, P. N. *Inorg. Chem.* **2014**, *53*, 679−681.
(19) Neofotistou, E.; Malliakas, C. D.; Trikalitis, P. N. *Chem.—Eur. J.* **2009**, *15*, 4523−4527.
(20) Schaate, A.; Roy, P.; Godt, A.; Lippke, J.; Waltz, F.; Wiebcke, M.; Behrens, P. *Chem.—Eur. J.* **2011**, *17*, 6643−6651.
(21) *APEX2 software package. Bruker Molecular Analysis Research Tool*, version 2008.4; Bruker AXS Inc.: Madison, WI, 2008.
(22) Sheldrick, G. M. *SADABS, Program for Absorption Correction of Area Detector Frames*; Bruker AXS Inc.: Madison, WI, 2001.
(23) *SCALE3 ABSPACK—An Oxford Diffraction program (1.0.4, gui:1.0.3) (C)*; Oxford Diffraction Ltd.: Oxford, U.K., 2005.
(24) Sheldrick, G. M. *SHELXTL 2008/4, Structure Determination Software Suite*; Bruker AXS Inc.: Madison, WI, 2008.
(25) Spek, A. L. *J. Appl. Crystallogr.* **2003**, *36*, 7−13.
(26) Myers, A. L.; Prausnitz, J. M. *AIChE. J.* **1965**, *11*, 121−127.
(27) DeCoste, J. B.; Peterson, G. W.; Jasuja, H.; Glover, T. G.; Huang, Y.; Walton, K. S. *J. Mater. Chem. A* **2013**, *1*, 5642−5650.
(28) Katz, M. J.; Brown, Z. J.; Colón, Y. J.; Siu, P. W.; Scheidt, K. A.; Snurr, R. Q.; Hupp, J. T.; Farha, O. K. *Chem. Commun.* **2013**, *49*, 9449−9451.
(29) The details of the computational strategies are provided in the SI.
(30) Cavenati, S.; Grande, C. A.; Rodrigues, A. E. *J. Chem. Eng. Data* **2004**, *49*, 1095−1101.
(31) Belmabkhout, Y.; Pirngruber, G.; Jolimaitre, E.; Methivier, A. *Adsorption* **2007**, *13*, 341−349.
(32) Krishna, R.; van Baten, J. M. *Phys. Chem. Chem. Phys.* **2011**, *13*, 10593−10616.
(33) He, Y.; Xiang, S.; Zhang, Z.; Xiong, S.; Wu, C.; Zhou, W.; Yildirim, T.; Krishna, R.; Chen, B. *J. Mater. Chem. A* **2013**, *1*, 2543−2551.
(34) Huang, H.; Zhang, W.; Liu, D.; Liu, B.; Chen, G.; Zhong, C. *Chem. Eng. Sci.* **2011**, *66*, 6297−6305.
(35) Banerjee, R.; Furukawa, H.; Britt, D.; Knobler, C.; O'Keeffe, M.; Yaghi, O. M. *J. Am. Chem. Soc.* **2009**, *131*, 3875−3877.
(36) Wang, B.; Côté, A. P.; Furukawa, H.; O'Keeffe, M.; Yaghi, O. M. *Nature* **2008**, *453*, 207−211.
(37) Yang, Q.; Zhong, C. *J. Phys. Chem. B* **2006**, *110*, 17776−17783.
(38) Cho, H.-Y.; Yang, D.-A.; Kim, J.; Jeong, S.-Y.; Ahn, W.-S. *Catal. Today* **2012**, *185*, 35−40.
(39) Demessence, A.; D'Alessandro, M. D.; Foo, M. L.; Long, J. R. *J. Am. Chem. Soc.* **2009**, *131*, 8784−8786.
(40) Bastin, L.; Bárcia, P. S.; Hurtado, E. J.; Silva, J. A. C.; Rodrigues, A. E.; Chen, B.-L. *J. Phys. Chem. C* **2008**, *112*, 1575−1581.
(41) Munusamy, K.; Sethia, G.; Patil, D. V.; Rallapalli, P. B. S.; Somani, R. S.; Bajaj, H. C. *Chem. Eng. J.* **2012**, *195*−*196*, 359−368.
(42) Kim, S.-N.; Kim, J.; Kim, H.-Y.; Cho, H.-Y.; Ahn, W.-S. *Catal. Today* **2013**, *204*, 85−93.
(43) Yang, Q.; Vaesen, S.; Vishnuvarthan, M.; Ragon, F.; Serre, C.; Vimont, A.; Daturi, M.; De Weireld, G.; Maurin, G. *J. Mater. Chem.* **2012**, *22*, 10210−10220.
(44) Huang, H.; Zhang, W.; Liu, D.; Zhong, C. *Ind. Eng. Chem. Res.* **2012**, *51*, 10031−10038.

dx.doi.org/10.1021/ic5013473 | *Inorg. Chem.* 2014, 53, 9254−9259